Proceedings of the ASME 2014 International Design Engineering Technical Conferences & Computers and Information in Engineering Conference
IDETC/CIE 2014
August 17-20, 2014, Buffalo, New York, USA

DETC2014-35123

AN INVERTED STRAIGHT LINE MECHANISM FOR AUGMENTING JOINT RANGE OF MOTION IN A HUMANOID ROBOT

Coleman Knabe
Virginia Tech
Blacksburg, Virginia, USA

Bryce Lee
Virginia Tech
Blacksburg, Virginia, USA

Dennis Hong, Ph.D.
University of California
Los Angeles, California, USA

ABSTRACT

Many robotic joints powered by linear actuators suffer from a loss of torque towards the limits of the range of motion. This paper presents the design of a fully backdriveable, force controllable rotary actuator package employed on the Tactical Hazardous Operations Robot (THOR). The assembly pairs a ball screw-driven linear Series Elastic Actuator (SEA) with a planar straight line mechanism. The mechanism is a novel inversion of a Hoeken's four-bar linkage, using the ball screw as a linear input to actuate the rotary joint. Link length ratios of the straight line mechanism have been chosen to optimize constant angular velocity, resulting in a nearly constant mechanical advantage and peak torque of 115 [Nm] throughout the 150° range of motion. Robust force control is accomplished through means of a lookup table, which is accurate to within ±0.62% of the nominal torque profile for any load case.

1. INTRODUCTION

The Tactical Hazardous Operations Robot (THOR), shown in Figure 1, is a full-size humanoid robot for rescue applications. Rescue tasks require not only a human-like range of motion in the lower body, but also a large amount of torque throughout those ranges. Having previously demonstrated the effectiveness of linear SEAs over force-controlled walking on the SAFFiR platform [1], the lower body of THOR is designed around a set of compact linear SEAs [2]. The hip and ankle joints connect the actuator output to a crank arm, which delivers peak torque near the nominal configuration [3]. Towards the limits of the range of motion, however, there is a significant decline in torque output as the mechanical advantage of the lever arm deteriorates. Since the knee and hip pitch joints require rotation exceeding 135°, as opposed to other joints which move up to 90°, achieving both range of motion and torque necessitated an innovative actuation strategy.

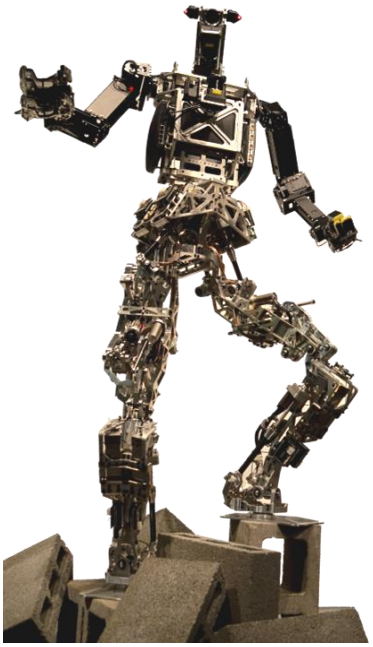

Figure 1: Tactical Hazardous Operations Robot (THOR)

While rotary SEAs can offer a constant torque profile and continuous rotation, designing two vastly different actuators was not appropriate considering the accelerated pace at which THOR was developed. Instead, a linear-to-rotary conversion mechanism was paired with the preexisting linear SEA. Several mechanisms were evaluated, including rack and pinions, slider cranks, cabling, and planar straight-line mechanisms such as the Watt, Chebyshev, Evans, Peauceillier-Lipkin, and Hoeken's linkages. Each of these linear-to-rotary convertors has its detriments, but an inverted Hoeken's four-bar linkage was best suited for this application due to its large crank angle range for a relatively short linear input.

The Hoeken's linkage, depicted in Figure 2, is a well-documented four-bar crank rocker mechanism typically used to approximate linear motion from a rotary input. Breen combines the linkage with a rotary motor to create an active vibration controller for automobile seats [4]. Barlas pairs two Hoeken's mechanisms to create a rocker-bogie transmission for a Mars rover suspension [5]. The end effector presented by Rodriguez features the linkage to realize 1-DOF planar actuation [6]. A number of other applications have used the Hoeken's linkage in a similar fashion [7-11].

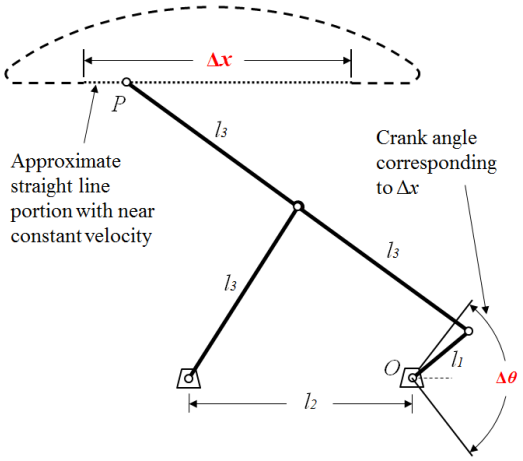

Figure 2: Hoeken's linkage schematic

The kinematics of the Hoeken's mechanism have been studied extensively [12-14], noting the tradeoff in linearity for constant velocity. For a given crank angle range, Norton provides a table of link length ratios optimized for either constant velocity or linearity in [12]. Bulatović optimizes both speed and linearity through the addition of an eccentricly geared crank input [14].

The mechanism in this paper follows optimized link length ratios detailed in Norton; however, it utilizes the Hoeken's linkage in an inverted configuration dissimilar to all previous applications. Section 2 of this paper overviews the design of the inverted mechanism and its incorporation into the thigh structure on THOR. Section 3 explores the implications of inverting the mechanism, specifically, the deviation in the torque profile resulting from cantilever deflection of the input SEA. Section 4 concludes the paper.

2. MECHANISM DESIGN

Hoeken's linkage synthesis and optimization is well documented and is not the focus of this paper. Instead, the design aspect for this application focused on providing a rigid structure for torque transmission and packaging the mechanism within the structure of the robot thigh. One four-bar was sized for use in both the knee and hip pitch joints, despite a variation in range of motion and mechanical interferences. The mechanism utilizes a ball screw-based linear SEA as the input of the Hoeken's linkage.

2.1 Linear Series Elastic Actuator

A set of compact, high-output linear SEAs were designed specifically for use on THOR. Figure 3 shows a CAD rendering of one of the actuators, displaying many of the essential components. A 100 [W] Maxon motor drives a precision ground ball screw through a 3:1 pulley ratio, delivering a peak output force of 2225 [N] at the ball nut. A Futek LCM200 tension/compression loadcell located in line with the actuator measures a load range of +/-2225 [N] at a resolution of +/-1 [N].

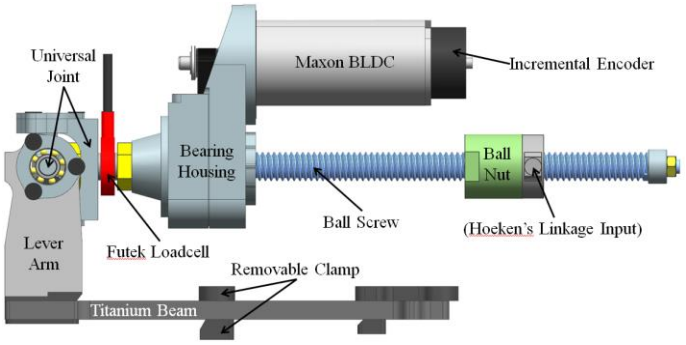

Figure 3: CAD rendering of Linear SEA employed in the lower body of THOR for the Hoeken's linkage

The elastic element is an evolutionary improvement on [16], mounting the a titanium cantilever beam parallel to the actuator. The compliance of the spring is configured through a removable clamp located halfway along the length of the beam, selecting the spring stiffness rate between a more stiff 650 [kN/m] or a more compliant 372 [kN/m].

The actuator is connected through a 2-DOF universal joint to a rigid lever arm on the beam, resulting in near perfect moment loading throughout the length of the beam. During operation, the cantilever bends under load, causing considerable deflection at the universal joint. An absolute optical encoder is located at each joint to compensate for the potentially detrimental effects of cantilever deflection on force control. Further details on the design of the THOR SEA can be found in [2].

2.2 Mechanism Packaging

For THOR, link length ratios were chosen from [12], to optimize the velocity of the linkage throughout a crank angle range of 150°. As with all crank-arm linkages, the torque output is linearly proportional to the length of the crank lever arm. Therefore, the crank arm was sized until the peak output torque corresponding to the SEA's 2225 [N] peak input reached the goal specification of 115 [Nm]. The resulting link lengths are given in Table 1.

Table 1: Link lengths of Hoeken's mechanism

l_1 (mm)	l_2 (mm)	l_3 (mm)	Δx (mm)
44.4	76	91.9	136.8

Through static analysis of the Hoeken's linkage, the force distribution within each link was calculated to determine bearing and link load requirements. Each joint in the linkage was loaded in double-shear to reduce individual bearing loads, prevent harmful torsion loads in the links, and assist in preloading the bearings to eliminate backlash. Many of the links are designed with a non-linear shape in order to avoid interferences throughout the range of motion. Figures 4 and 5 show the side and front views, respectively, of the Hoeken's linkage in the knee and hip pitch joints.

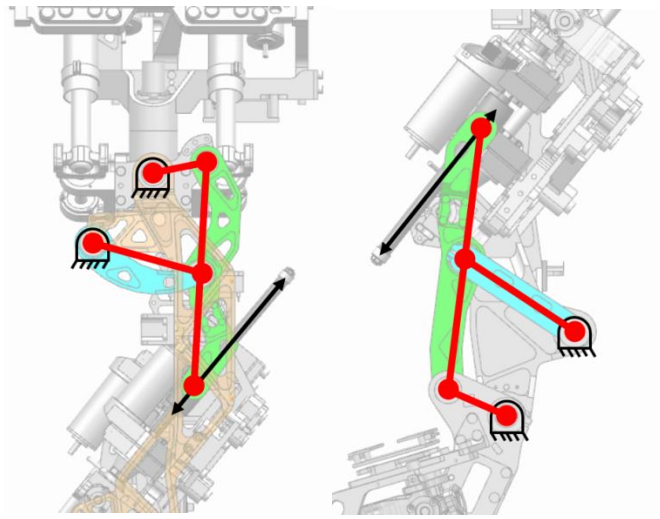

(A) (B)

Figure 4: Side views of Hoeken's mechanism in its nominal configuration packaged within thigh for the hip pitch (A) and knee pitch (B) joints, overlain with a schematic of the Hoeken's linkage

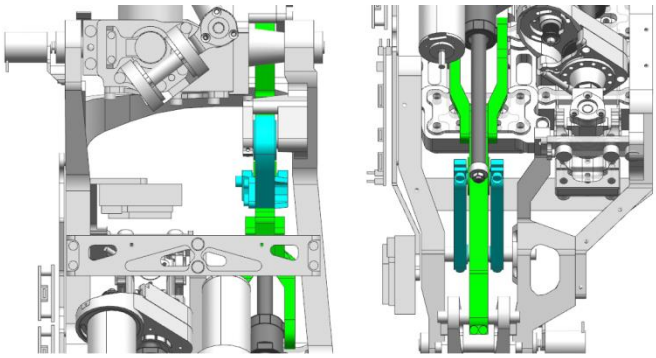

(A) (B)

Figure 5: Front views of Hoeken's mechanism for the hip pitch (A) and knee pitch (B) joints

The width of the hip joint is greatly dependent on the width of the hip pitch linkage, so design efforts focused on reducing the width of the hip linkage to less than the width of the SEA: 0.041 [m]. Making the hip linkage thin results in increased difficulty of repairs, as essentially the entire leg must be dismantled to replace any part. The width of the knee linkage is wider, 0.065 [m], allowing for easier repairs through removal of the bearing shafts. Though the final rotary packages are quite thin, they occupy a large area footprint. For this reason, they cannot be used in other joints.

Figures 6 and 7 display the motion of the linkage through the hip pitch and knee ranges of motion, respectively. The hip pitch linkage produces joint motion from -120° to +30°. Though the knee linkage is designed for 150° of crank rotation, structural interferences between the calf and thigh reduced the knee joint rotation to 135°.

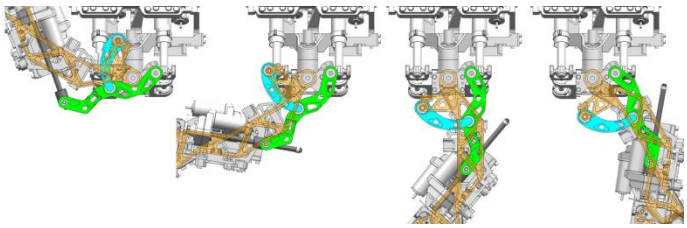

Figure 6: Hip pitch Hoeken's linkage at -120°, -60°, 0°, and 30°

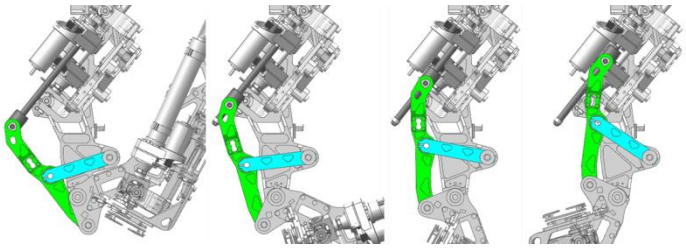

Figure 7: Knee Hoeken's linkage at 135°, 90°, 45°, and 0°

The addition of the inverted Hoeken's linkage to the SEA successfully augments the output joint range of motion to 150°. Kinematic analysis indicates a linearity error of less than 1% with an output angular velocity error of 4.25%. Since the actuator is supported through a universal joint on one side, the actuator can pitch and roll to accommodate linearity errors and compensates for any variance in the machining or assembly process.

3. TORQUE ERROR ANALYSIS

The angular velocity and linearity errors intrinsic to the Hoeken's linkage create a small deviation in the mechanical advantage of the mechanism along its range of motion. Furthermore, cantilever deflection under load introduces deviation from the nominal torque output curve. A mechanical advantage lookup table is used to compute nominal feedforward joint torques from measured joint angle. Coupling data from the in-line loadcell and an absolute optical encoder at the output joint enable robust force control of the knee and hip pitch joints.

Despite actuator linear displacement being the input to the Hoeken's linkage, proprioceptive data obtained from the absolute joint encoder and loadcell greatly simplify calculations for the torque profile. Therefore, all derivations are functions of these sensor readings. Figure 8 shows the knee rotary actuator package overlaid with the schematic used for calculations in this section. Calculations are based on a generic crank angle,

which are phase shifted for use on the knee and hip pitch joints depending on their nominal configuration on THOR.

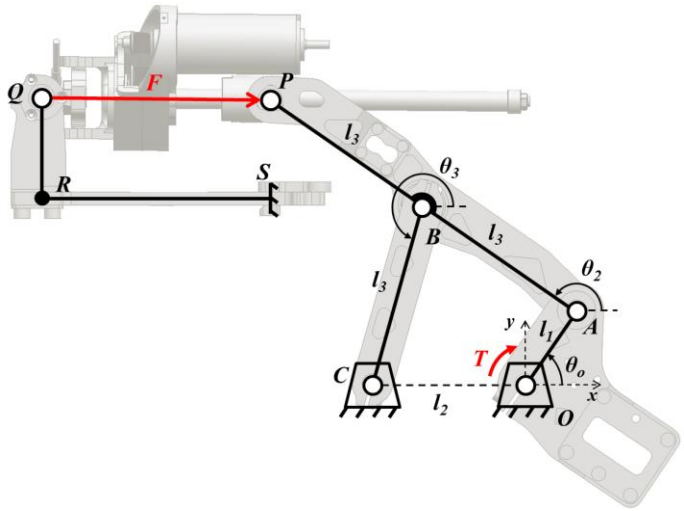

Figure 8: Schematic of SEA and Hoeken's linkage overlaid on knee joint

3.1 Nominal Mechanical Advantage Profile

To generate the lookup table for computing feedforward joint torques, the Hoeken's linkage was decoupled from the actuator, and a generalized force vector along $\overrightarrow{QP}$ was used as the input. Position analyses for Hoeken's linkages are ubiquitous and are not the focus of this paper. Figure 9 displays the free-body diagram (FBD) of the linkage.

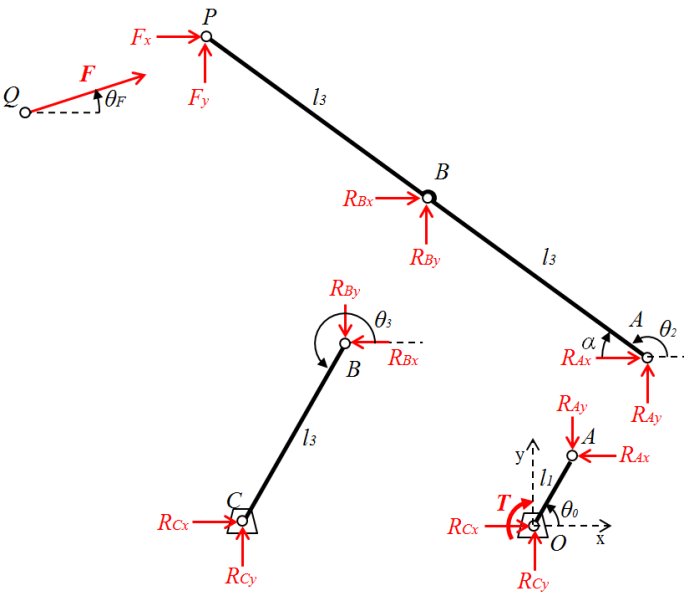

Figure 9: Free body diagram of Hoeken's linkage

Summing horizontal and vertical forces in link *AP* reveals:

$$R_{Ax} = -F_x - R_{Bx} = -F\cos\theta_F - R_{Bx} \quad (1)$$

$$R_{Ay} = -F_y - R_{By} = -F\sin\theta_F - R_{By} \quad (2)$$

Summing moments in link *AP* about point *A* gives:

$$\sin\alpha\,(2F_x + R_{Bx}) + \cos\alpha\,(2F_y + R_{By}) = 0 \quad (3)$$

Since link *BC* is a two-force member:

$$R_{By} = R_{Bx}\tan\theta_3 \quad (4)$$

Combining equations 1-4 gives solutions for the reaction forces at joint *A*,

$$R_{Ax} = -F\cos\theta_F + 2F\frac{\sin\alpha\cos\theta_F + \cos\alpha\sin\theta_F}{\sin\alpha + \cos\alpha\tan\theta_3} \quad (5)$$

$$R_{Ay} = -F\sin\theta_F + 2F\frac{\sin\alpha\cos\theta_F + \cos\alpha\sin\theta_F}{\sin\alpha + \cos\alpha\tan\theta_3}\tan\theta_3 \quad (6)$$

where θ_F is the angle at which force is applied to point P. Summing moments in link *AO* about point *O* gives:

$$T = l_1\left(R_{Ax}\sin\theta_0 - R_{Ay}\cos\theta_0\right) \quad (7)$$

Substitution of (5) and (6) into (7) results in a solution for output torque as a function of known joint angles and an input force along $\overrightarrow{QP}$. This solution holds true for crank angles between -90° and +90°. The nominal coordinates for point *Q* on THOR are (-0.2391 [m], 0.1413 [m]) from the output joint, *O*. Figure 10 shows the nominal mechanical advantage profile across a crank angle range of 150° using link lengths from Table 1.

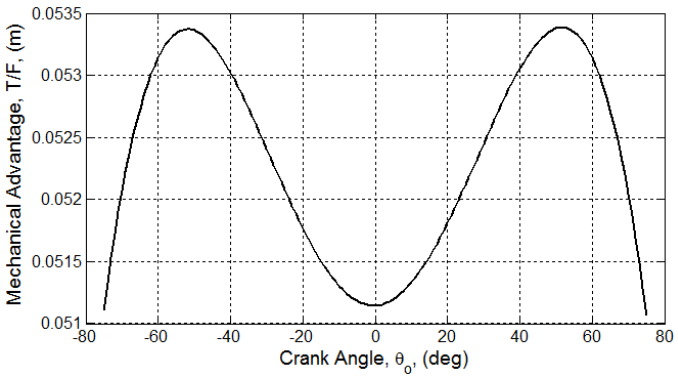

Figure 10: Nominal mechanical advantage profile of THOR Hoeken's linkage

Since the feedforward torque is computed using the nominal mechanical advantage lookup table, torque errors arise from deflection of the cantilever beam under load. A 2-dimensional lookup table based on both force input and joint angle could compensate for these errors, at the tradeoff of

computational performance. While the 1-dimensional lookup table can easily be handled by the custom motor controllers, it is imperative to know worst-case deviation from nominal mechanical advantage prior to committing to the use of a 2-dimensional lookup table.

3.2 Mechanical Advantage with Cantilever Deflection

The percentage deviation from the nominal mechanical advantage profile was computed using the derivations from Section 3.1 after determining worst-case deflection of point *Q* from a simplified cantilever beam model. To approximate the displacement at the output lever arm, the titanium spring was treated as a cantilever loaded by a pure moment at point *R*, equivalent to Fh. Figure 11 depicts the load case of a cantilever beam in moment. This model assumes that the force is applied horizontally at point *Q*.

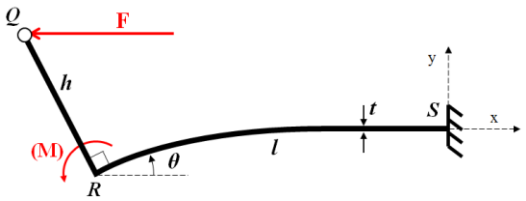

Figure 11: Load case for cantilever spring deflection

The equations for maximum deflection and slope at the end of a beam in moment are:

$$y_R = -\frac{Ml^2}{2EI} \tag{8}$$

$$\theta_R = \frac{Ml}{EI} \tag{9}$$

Therefore, the deflection of point *Q* from its nominal configuration is described by equations 10 and 11.

$$\Delta Q_x = -h \sin\theta_R = -h \sin\frac{Fhl}{EI} \tag{10}$$

$$\Delta Q_y = y_R + h\,(\cos\theta_R - 1) = \frac{-Fhl^2}{2EI} + h\,(\cos\frac{Fhl}{EI} - 1) \tag{11}$$

The compliant beam employed on THOR is made of Ti-6Al-4V. Dimensions of the beam in its most compliant setting are given in Table 2.

Table 2: Dimensions of THOR compliant beam

l (m)	*w* (m)	*t* (m)	*h* (m)
0.0551	0.0380	0.0065	0.05

Using equations 10 and 11, deflections of point *Q* were calculated for the two worst-case loading scenarios: peak actuator forces of +2225 [N] and -2225 [N]. The mechanical advantage profiles were recalculated, incorporating the resulting cantilever deflections. Figure 12 shows the percent error that these two cases deviate from the nominal mechanical advantage profile.

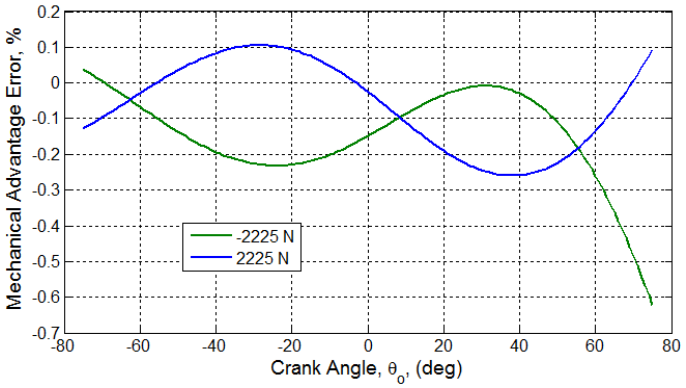

Figure 12: Percentage deviation from nominal mechanical advantage profile due to worst-case cantilever deflection

The mechanical advantage error stays within ±0.25% for the majority of the range of motion, and only exceeds this at the end of the motion. The maximum deviation from the nominal profile is -0.62%, which occurs at maximum joint deflection. Therefore, feedforward torque compensation can be accomplished using a single mechanical advantage lookup table without any significant loss in performance.

4. CONCLUSIONS

This paper presents the design of a novel linear-to-rotary conversion mechanism used to achieve a large joint range of motion with consistently high torque for a humanoid robot THOR. An inverted Hoeken's four-bar straight line approximator was coupled with the output of a ball screw-driven linear SEA, creating a backdriveable, force-controllable rotary assembly. The resulting actuator has a nearly constant mechanical advantage, and produces a peak torque of 115 [Nm] throughout the 150° range of motion.

The rotary actuator has been incorporated into the knee and hip pitch joints on THOR, enabling ranges of motion from 0° to 135° and -120° to 30°, respectively. Robust force control is achieved by means of a mechanical advantage lookup table in tandem with proprioceptive data from a loadcell and absolute joint encoder. Cantilever beam deflection intrinsic to the SEA compliant element introduces a -0.62% maximum deviation from the nominal mechanical advantage profile, which is insignificant for force control applications.

While the design presented in this paper is exclusive to THOR, the concept of an inverted Hoeken's mechanism may be applied to other mechanical systems in demand of a linear-to-rotary converter. Future work with the THOR rotary actuator includes analysis into the effects that link flexure and joint backlash may have on joint force control. The authors have developed a custom actuator test stand to enable this investigation.

ACKNOWLEDGMENTS

This work is supported by DARPA through grant N65236-12-1-1002 and by ONR through grant N00014-11-1-0074.

REFERENCES

[1] Lahr, D., Orekhov, V., Lee, B., and Hong, D., "Development of a Parallely Actuated Humanoid, SAFFiR". Proceedings of the ASME International Design Engineering Technical Conferences & Computers and Information in Engineering Conference, 2013.

[2] Knabe, C., Lee, B., Orekhov, V., and Hong, D., "Design of a Compact, Lightweight, Electromechanical Linear Series Elastic Actuator". Proceedings of the ASME International Design Engineering Technical Conferences & Computers and Information in Engineering Conference, 2014.

[3] Lee, B., Knabe, C., Orekhov, V., and Hong, D., "Design of a Human-Like Range of Motion Hip Joint for Humanoid Robots". Proceedings of the ASME International Design Engineering Technical Conferences & Computers and Information in Engineering Conference, 2014.

[4] Breen, J. and Hayner, M., "Actuator Including Mechanism for Converting Rotary Motion to Linear Motion," U.S. Patent 8 360 387, Jan. 29, 2013.

[5] Barlas, F., "Design of a Mars Rover Suspension Mechanism," M.S. thesis, Dept. Mech. Eng., Izmir Inst. of Technology, Izmir, Turkey, 2004.

[6] Rodriguez, A., and Mason, M. T., "Effector Form Design for 1DOF Planar Actuation". Proceedings of the IEEE International Conference on Robotics and Automation, 2013.

[7] Lu, S., Zlatanov, D., Ding, X., and Molfino, R., "A New Family of Deployable Mechanisms Based on the Hoeken's Linkage". Mechanism and Machine Theory, Vol. 73, pp. 130–153, 2014.

[8] Barb, L., Piccin, O., Gangloff, J., Bayle, B., and Rump, R., "Design of a Linear Haptic Display Based on Approximate Straight Line Mechanisms". Proceedings of IEEE International Conference on Intelligent Robots and Systems, pp. 5048–5053, 2010.

[9] Saha, S. K., Prasad, R., and Mandal, A. K., "Use of Hoeken's and Pantograph Mechanisms for Carpet Scrapping Operations". Proceedings of the 11th National Conference on Machines and Mechanisms, pp. 732–738, 2003.

[10] Fremgen, B., "Atrophy-Reducing Movable Foot Support Apparatus". U.S. Patent 7 922 187, Apr. 12, 2011.

[11] Beroz, J., Awtar, S., and Hart, A. J, "Extensible-Link Kinematic Model for Determining Motion Characteristics of Compliant Mechanisms". Proceedings of the ASME International Design Engineering Technical Conferences & Computers and Information in Engineering Conference, 2013.

[12] Norton, R., *Design of Machinery*, 4th ed. Boston: McGraw Hill, 2008, pp. 140-145.

[13] Norton, R., "In Search of the 'Perfect' Straight Line and Constant Velocity Too". Proceedings of the 6th Applied Mechanisms and Robotics Conference, 1999.

[14] Bulatović, R. and Dordević, S., "On the Optimum Synthesis of a Four-Bar Linkage Using Differential Evolution and Method of Variable Controlled Deviations". Mechanism and Machine Theory, Vol. 44, pp. 235–246, 2009.

[15] Huang, Z., Du, Y., Yu, W., Qi, X., Yang, Z., and Lang, Q., "Kinematic Characteristics and Optimization Analysis of Oval Geared Hoeken Mechanism". Applied Mechanics and Materials, Vols. 215-216, pp. 9–13, 2012.

[16] Orekhov, V., Lahr, D., Lee, B., and Hong, D., "Configurable Compliance for Series Elastic Actuators". Proceedings of the ASME International Design Engineering Technical Conferences & Computers and Information in Engineering Conference, 2013.